Proceedings World Geothermal Congress 2026
Calgary, Canada, June 8 – 11, 2026

Application of a physics-informed neural network for inverse modeling of natural-state geothermal reservoir

Kazuya Ishitsuka[1]*, Keiichi Ishizu[2], Norihiro Watanabe[3], Yusuke Yamaya[3], Anna Suzuki[4], and Yusuke Ohta[5]

Kyoto University[1]*, Kyushu University[2], National Institute of Advanced Industrial Science and Technology[3] , Tohoku University[4] , Japan Agency for Marine-Earth Science and Technology[5]

ishitsuka.kazuya.4w@kyoto-u.ac.jp

Keywords: Physics-informed neural networks, Inverse modeling, Natural-state simulation, Magnetitellurics, Permeability

1 INTRODUCTION

Natural-state reservoir simulation is a gold standard approach in modeling geothermal systems. Based on a conceptual model of the target geothermal field, an optimal numerical model of natural conditions is created by performing simulations that are consistent with well logs. Various methods including iterative optimization algorithms (Bjarkason et al., 2019) and Bayesian approaches (Scott et al., 2022) have been developed to calibrate natural-state simulations. Although these methods have been shown to be effective for inverse modeling of natural-state model, improvements are needed regarding the efficiency of unknown parameter exploration and computational cost.

Recent developments in machine learning have led to a research area called scientific machine learning (SciML). SciML aims to combine existing scientific approaches with data-driven machine learning to generate new scientific knowledge. Physics-informed neural networks (PINNs) are one of the central methods in SciML. This method enables to obtain predictions that satisfy physical laws by incorporating partial differential equations into the loss function of the neural network (Raissi et al., 2019). PINNs uses automatic differentiation (AD) to calculate derivatives in partial differential equations. In standard numerical schemes such as finite element and finite difference, derivatives calculated based on finite meshes, and it is inevitable that calculated derivatives contain rounding and truncation errors. Derivative calculation by AD does not require a mesh; instead, it constructs a computational graph and utilizes the chain rule to compute derivatives, thereby achieving accurate derivative computation.

By taking the advantage of seamless integration of data and physics and accurate calculation of gradients, recent studies have utilized PINNs to improve the inverse problems in geothermal development. For example, Ishitsuka et al. (2023) has demonstrated the effectiveness of PINNs for inverse modeling of natural-state geothermal systems. Qin et al. (2024) showed the usefulness of PINNs for learning energy production of time-series data, and Yan et al. (2024) predicted system behavior in enhanced geothermal systems by PINNs. Aljubran and Horne (2024) estimated 3D subsurface temperatures in the United States using PINNs. Shima et al. (2024) showed that unobserved geothermal structures were predicted by utilizing transfer learning of PINNs. Ishitsuka et al. (2025) examined learning strategies of PINNs and demonstrated effectiveness of PINNs for 3D natural-state geothermal modeling by integrating well logs and magnetotelluric (MT) data.

In this study, we applied the method of Ishitsuka et al. (2025) to the 3D natural-state geothermal model of Dimou et al. (2024) and examined its characteristics in inverse modeling. The numerical model by Dimou et al. (2024) was constructed based on the geothermal reservoir of the Ogiri geothermal field located south of Japan. Based on the synthetic well data created from the model, we predicted the spatial distribution of temperature, fluid pressure, and permeability using the PINN. Furthermore, we investigated a method applying transfer learning as a way to incorporate expert knowledge about the permeability structure into the PINN. In addition, we examined a method for refining permeability structures by integrating MT data and well data using the PINN.

2 METHOD AND DATASET

2.1 Physics-informed neural networks for inverse modeling of natural-state geothermal systems

2.1.1 Inverse modeling based on well data

A standard neural network considered the misfit between observations and network outputs in loss function (L_{data}), and network training is performed to minimize the loss function. In PINNs, in addition to the data misfit

(L_{data}), inconsistencies with physical laws ($L_{physics}$) and boundary conditions ($L_{boundary}$) are incorporated into the loss function of the neural network. Thus, PINNs train neural networks to satisfy physical laws and boundary conditions.

$$LOSS = L_{\text{data}} + L_{\text{physics}} + L_{\text{boundary}} \tag{1}$$

In this study, we considered steady-state mass and energy conservation laws as a loss function (L_{mass} and L_{energy}).

$$L_{\text{physics}} = \alpha|L_{\text{mass}}| + \beta\left|L_{\text{energy}}\right| \tag{2}$$

Here, $L_{\text{mass}} = \nabla \cdot \left(\rho_f v\right)$ and $L_{\text{energy}} = \nabla \cdot \left(\rho_f H v\right) - \nabla \cdot \lambda \nabla T$. ρ_f and λ indicate fluid density and bulk rock thermal conductivity, respectively. H and T are specific enthalpy and temperature, respectively. v is darcy velocity and described as $v = -\frac{K}{\mu_f}\left(\nabla P - \rho_f g \nabla z\right)$. Here, P is fluid pressure. K, μ_f and g are permeability, fluid viscosity and gravity acceleration, respectively. We considered pure water as pore fluid for simplicity. ρ_f, c_f, and μ_f are temperature and pressure dependent variables, and these fluid properties were calculated according to IAPWS-IF97 formula. $\nabla z = 1$ in vertical direction; otherwise, $\nabla z = 0$. Bulk rock thermal conductivity was set to be constant for simplicity.

As a network architecture, we used three fully connected neural network. Each network has an input of coordinates and outputs are either temperature (T), pressure (P), or logarithm of permeability (K). These three networks are mutually influenced as loss component for physical laws and boundary conditions use all these physical quantities. The network was trained over 30,000 epochs using Adam optimizer with a piece wise decay learning rate. In the coupled condition of heat and fluid transfer, the balance of the mass and energy loss components (α and β) influence the training performance. This study used the coefficient annealing strategy proposed by Wang et al. (2021) to adaptively determine α and β.

When well locations are unevenly distributed, prediction of the target permeability structure based solely on well data is expected to be difficult. Ishitsuka et al. (2025) and Shima et al. (2024) proposed a method to refine the permeability structure by applying transfer learning to the PINN. Specifically, the PINN is firstly pre-trained on a simplified numerical model of the target permeability structure. Fine-tuning of the network is then performed by transfer learning (TL) of the trained PINNs to well data. In this study, we applied the transfer learning strategies and compared the results with those obtained without transfer learning. Fine-tuning was performed by learning the network parameters of the layer closest to the output while fixing the parameters of all other layers. The approach is called as the PINN-TL in the following.

2.1.2 Inverse modeling based on well data and magnetotelluric data

MT is a passive exploration technique that measures the fluctuation of natural electric ($\boldsymbol{E}$) and magnetic ($\boldsymbol{H}$) field at the surface of the Earth and determines the resistivity structure at depth. Resistivity structures obtained by MT method have been used to interpret geothermal structures (Yamaya et al., 2022). In the MT method, horizontal electric and magnetic field over time are converted to frequency domain, and the relationship between the fields are described by impedance tensor ($\boldsymbol{Z}$) given by $\boldsymbol{E} = \boldsymbol{Z}\boldsymbol{H}$. The impedance tensor is complex and has real ($\boldsymbol{X}$) and imaginary parts ($\boldsymbol{Y}$) as $\boldsymbol{Z} = \boldsymbol{X} + i\boldsymbol{Y}$. Apparent resistivity $\rho_{ij}^{a} = \frac{1}{\mu\omega}\left|\frac{\boldsymbol{E_i}}{\boldsymbol{H_j}}\right|^2$ as a function of frequency (f) is calculated from the electric and magnetic field. Here, ω indicates angular frequency ($\omega = 2\pi f$) and μ is magnetic permeability. i and j are either x (north-south) and y (east-west) direction. Phase is represented as $\boldsymbol{\phi} = \boldsymbol{X}^{-1}\boldsymbol{Y}$. Both apparent resistivity and phase have four components (xy, yx, xx, and yy). This study considered xy and yx components because the magnitudes of these components are much larger than those of xx and yy components in the numerical model.

We considered 100 MT observation sites on the ground surface of the numerical model and assumed 11 frequencies from 10^{-4} to 10^{3} Hz. The forward MT simulation was implemented based on Ishizu et al. (2022). Reference resistivity was calculated rock physics models from temperature, pressure, and permeability. For fluid resistivity, the equation by Watanabe et al. (2021) was used. When MT data is incorporated into the inverse modeling by the PINN, the loss representing the discrepancy between reference and predicted MT responses were added to the loss. In this study, following the method of Ishitsuka et al. (2025), we first trained the PINN on well data alone to learn temperature, pressure, and permeability fields. Subsequently, we fixed the network parameters predicting temperature and pressure and trained the network parameters for permeability using both well data and MT data.

2.2 Numerical datasets used in this study

The Ogiri geothermal field lies in the western slope of the Kirishima volcano, one of the largest quaternary volcanoes in the southwestern Japan (Goko, 2000). Andesite lava and pyroclastic rocks associated with extensive volcanic activity during the Pleistocene are distributed from near the surface to a depth of about 2000 m overlying pre-Neogene basement rocks consisting mainly of sandstone and shale. Main faults have been identified along the NE-SE and ENE-WSW directions, and surface geothermal signatures such as fumaroles, hot springs, and hydrothermal alteration effects have been identified along these faults (Goko, 2000). Dimou et al. (2024) constructed the permeability structure of the numerical model for the main fault-controlled type. Natural-state simulation was performed using TOUGH2 (Pruess, 2004). The computational domain of the simulation has 8 km×10 km in horizontal space and 2.3 km in depth direction with mesh grid of 19×20×22 (Dimou et al., 2024). As described in Dimou et al. (2024), the numerical model was not created to accurately reproduce the Ogiri geothermal field, but to construct a representative model for a fault-controlled geothermal reservoir. This study focused on a central region of the numerical model, approximately 4.4 km×4.6 km×2.3 km (17×16×22 mesh grid).

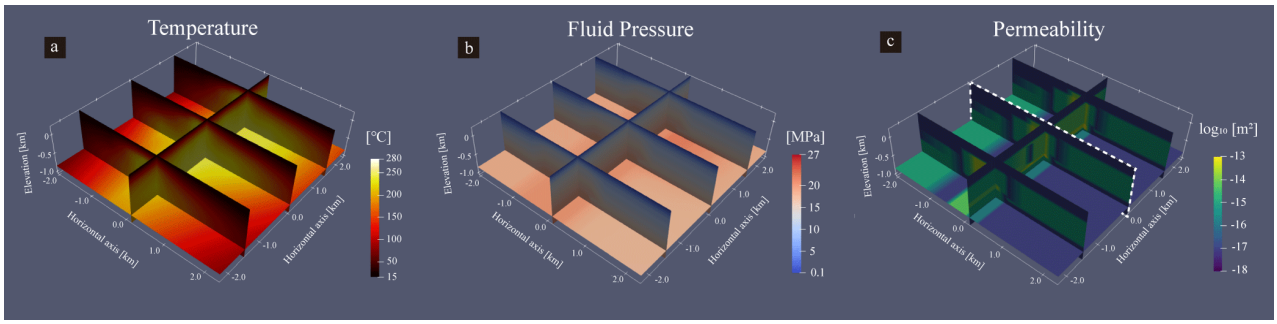


Figure 1. (a) Temperature, (b) fluid pressure, and (c) permeability of the reference numerical model used in this study. The white dashed rectangle in (c) indicates the location of the cross-section of Figures 3 and 4c.

3 RESULTS AND DISCUSSION

3.1 Comparison with data-driven machine learning approaches

Figure 2 is the average absolute errors of temperature, fluid pressure, and permeability predicted by the proposed PINN, neural network (NN), extreme gradient boosting (XGB), and ordinary kriging (OK). The boxplots were obtained from five runs with different well locations. The mean and median errors in temperature and pressure predicted by the PINN were smaller than those predicted by other data-driven methods (Figure 2). Since the architecture of the neural network used in this comparison is the same as that of the PINN, the differences in the prediction errors between the PINN and NN are attributed to the incorporation of physical laws and boundary conditions. Compared to the pressure error, the temperature error showed a greater benefit from the PINN. The error in permeability was reduced by using the PINN compared to NN (Figure 2c). Ishitsuka et al. (2025) showed that the accuracy improvement in permeability prediction achieved by using PINN was small. However, based on Figure 2c, the impact of the PINN on enhancing prediction accuracy of permeability may vary depending on the permeability structure and data being analyzed. Considering the errors in temperature, pressure, and permeability, the PINN exhibited superior predictive performance compared to other data-driven methods (Figure 2). In addition, the streamline characteristics calculated from temperature and pressure based on reference data and predictions were consistent with each other. Geothermal fluids formed an upward flow along the high-temperature and high-permeability zone, and the mass flow rate of this upward flow was greater than in the surrounding areas.

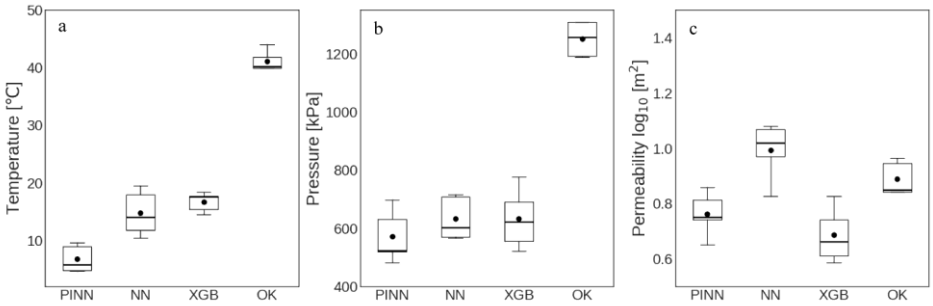


Figure 2. Average absolute errors in (a) temperature, (b) pressure, and (c) permeability modeled by the proposed physics-informed neural network (PINNs), neural network (NN), extreme gradient boosting (XGB), and ordinary kriging (OK). Black dots and lines indicate mean and median values, respectively.

3.2 Permeability refinement by the physics-informed neural network with transfer learning

Figure 3 indicates permeability structure of the reference numerical model and those predicted by the PINN and PINN-TL. For the PINN-TL, simplified permeability structure shown in Figure 3c was created based on the reference permeability. More specifically, the prior permeability model was created as a prior data by substituting the reference permeability values. Therefore, the shape of the prior permeability is similar to that of the reference permeability, but the values differ (Figure 3a and 3c). When creating prior permeability for the application of the PINN targeting actual fields, it would be possible to integrate geological, geophysical, and geochemical data to build an approximate permeability structure based on expert knowledge. The permeability obtained from well data using the PINN without a prior permeability model predicted the overall permeability structure well, but the structural boundaries of the permeability were unclear (Figure 3b). In contrast, by the PINN-TL, a permeability structure with sharp boundaries was modeled (Figure 3d). The magnitude of permeability obtained from the PINN-TL were not exactly same as the prior permeability, indicating that prior permeability was modified based on well data and physics information by the PINN-TL (Figure 3c and 3d).

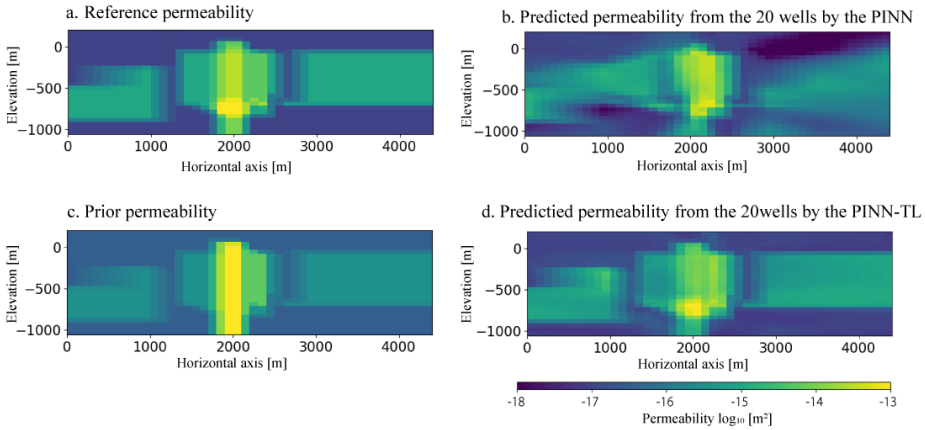


Figure 3. Permeability along the cross-section shown in Figure 1c. (a) Permeability of the reference model, (b) permeability predicted from the 20 wells by the physics-informed neural network (PINN), (c) prior permeability model used at the pre-training step in the transfer learning strategy, and (d) permeability predicted from 20 wells by the physics-informed neural network with transfer learning (PINN-TL).

3.3 Permeability refinement by incorporating magnetotelluric data into the physics-informed neural network

By incorporating the discrepancy between reference and predicted MT data, the loss component for permeability reduced. Accordingly, the training loss was reduced over epoch. The predicted MT data generally matched the reference MT data (Figure 5a and 5b), and significant permeability refinement was found as shown in Figure 5c. Permeability has improved, particularly in high-permeability zones (Figure 5c). In general, the high permeability zone exhibits relatively high sensitivity in MT data compared to low-permeability zones. The permeable zone governs the flow of geothermal fluids; therefore, refining the shape and magnitude of permeability at the zone is expected to significantly contribute to improving numerical models of geothermal reservoirs. This result demonstrates that the PINN enables the refinement of geothermal reservoir models by integrating different types of data—well data and MT data.

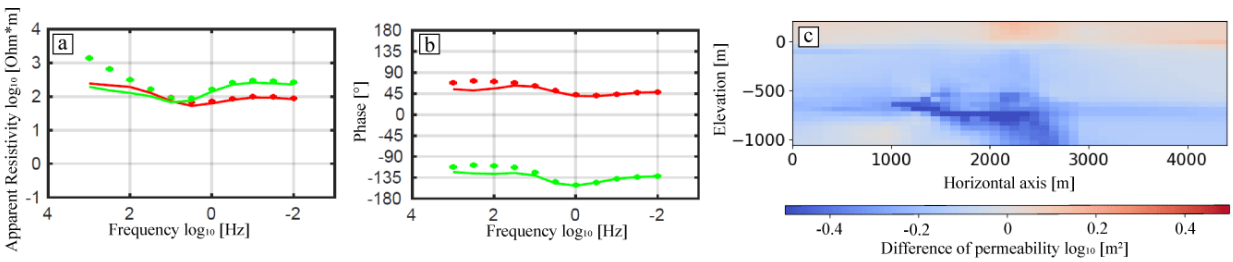


Figure 4. Example of reference and predicted magnetotelluric data: (a) apparent resistivity and (b) phase. Dots and lines indicate reference and predicted values, respectively. Red and green colors correspond to xy and yx components, respectively. (c) The difference between the permeability predicted from well data and MT data and the permeability predicted from well data.

Acknowledgements

This study is based partly on the results obtained from a project, JPNP21001, commissioned by the New Energy and Industrial Technology Development Organization (NEDO), Japan. Kazuya Ishitsuka was also funded by the Japan Society for the Promotion of Science (JSPS) KAKENHI (Grant JP23K26601). Kazuya Ishitsuka and Anna Suzuki also acknowledge the support by the Japan Society for the Promotion Science for the Grant-in-Aid for Transformative Research Areas (A), "Establishing data descriptive science and its cross-disciplinary applications" (Grant JP22H5108).

REFERENCES <HEADING STYLE>

Aljubran, M. J., and Horne, R. N.: Thermal Earth model for the conterminous United States using an interpolative physics-informed graph neural networks, *Geothermal Energy*, **12**, (2024), 25.

Bjarkason, E. K., O'Sullivan, J. P., Yeh, A., and O'Sullivan, M. J.: Inverse modeling of the natural state of geothermal reservoirs using adjoint and direct methods, *Geothermics*, **78**, (2019), 85-100.

Dimou, A. P., Suzuki, A., and Ohta, Y.: Benchmark datasets of representative geothermal reservoir models with pseudo-geophysical exploration and well data, *Data in Brief*, **56**, (2024), 110828.

Goko, K.: Structure and hydrology of the Ogiri field, West Kirihima geothermal area, Kyushu, Japan, *Geothermics*, **29**, (2000), 127-149.

Ishitsuka, K., Ishizu, K., Watanabe, N., Yamaya, Y., Suzuki, A., Bandai, T., Ohta, Y., Mogi, T., Asanuma, H., Kajiwara, T., and Sugimoto, T.: Reliable and practical inverse modeling of natural-state geothermal systems using physics-informed neural networks: three-dimensional model construction and assimilation with magnetotelluric data, *Journal of Geophysical Research: Machine Learning and Computation*, **2**, (2025), e2025JH000683.

Ishitsuka, K., and Lin, W.: Physics-informed neural network for inverse modeling of natural-state geothermal systems, *Applied Energy*, **337**, (2023), 120855.

Ishizu, K., Siripunvaraporn, W., Goto, T., Koike, K., Kasaya, T., and Iwamoto, H.: A cost-effective three-dimensional marine controlled-source electromagnetic survey: Exploring seafloor massive sulfides, *Geophysics*, **87**(4), (2022), E219-E241.

Pruess, K.: The TOUGH codes – a family of simulation tools for multiphase flow and transport processes in permeable media, *Vadose Zone Journal*, **3**(3), (2004),738-746.

Qin, Z., Jiang, A., Faulder, D., Cladouhos, T. T., and Jafarpour, B.: Physics-guided deep learning for prediction of energy production from geothermal reservoirs, *Geothermics*, **116**, (2024), 102824.

Raissi, M., Perdikaris, P., and Karniadakis, G. E.: Physics-informed neural networks: A deep learning framework for solving forward and inverse problems involving nonlinear partial differential equations. *Journal of Computational Physics*, **378**, (2019) 686–707.

Scott, S. W., O'Sullivan, J. P., Maclaren, O. J., Nicholson, R., Covell, C., Newson, J., and Guðjónsdóttir, M. S.: Bayesian calibration of a natural state geothermal reservoir model, Krafla, north Iceland, *Water Resources Research*, **58**, (2022), e2021WR031254.

Shima, A., Ishitsuka, K., Lin, W., Bjarkason, E. K., and Suzuki, A.: Modeling unobserved geothermal structures using a physics-informed neural network with transfer learning of prior knowledge, *Geothermal Energy*, **12**, (2024), 38.

Wang, S., Teng, Y., and Perdikaris, P.: Understanding and mitigating gradient flow pathologies in physics-informed neural networks, *SIAM Journal on Scientific Computing*, **43**, (2021), A3055-A3081.

Watanabe, N., Yamaya, Y., Kitamura, K., and Mogi, T.: Viscosity-dependent empirical formula for electrical conductivity of H2O-NaCl fluids at elevated temperatures and high salinity, *Fluid Phase Equilibria*, **549**, (2021), 113187.

Yamaya, Y., Suzuki, Y., Murata, Y., Okamoto, K., Watanabe, N., Asanuma, H., Hase, H., Ogawa, Y., Mogi, T., Ishizu, K., and Uchida, T.: 3-D resistivity imaging of the supercritical geothermal system in the Sengan geothermal region, NE Japan, *Geothermics*, **103**, (2022), 102412.

Yan, B., Gudala, M., Hoteit, H., Sun, S., Wang, W., and Jiang, L.: Physics-informed machine learning for noniterative optimization in geothermal energy recovery, *Applied Energy*, **365**, (2024), 1213179.